Spin-polarization dependence of the Rb-Xe spin-exchange optical pumping process

Bowen Song,[1] Yanhua Wang,[2,1] and Nan Zhao[1,*]

[1]*Beijing Computational Science Research Center, Beijing 100193, People's Republic of China*

[2]*School of Physics and Electronic Enginering, Shanxi University, Taiyuan 030006, People's Republic of China*

(Received 28 January 2021; accepted 27 July 2021; published 17 August 2021)

We experimentally study the Rb-Xe spin-exchange optical pumping process. The dependence of the spin-exchange rate on the intensity of the pumping light is measured at different temperatures under low magnetic fields. We demonstrate that the spin-exchange rate will decrease as the Rb spin polarization increases, which agrees well with the theoretical prediction. In our measurement, three spin exchange and spin relaxation mechanisms, namely, the spin exchange rates between Rb and Xe atoms caused by van der Waals molecule (Γ_{vdW}) and binary collision (Γ_{bin}) processes, and the spin relaxation rate due to the wall collision of Xe atoms (Γ_w), have comparable magnitudes. These rates are extracted separately from the measured data with different Rb spin polarization at various temperatures. Our work provides a comprehensive confirmation of the physical picture of the spin-exchange optical pumping process.

DOI: 10.1103/PhysRevA.104.023105

I. INTRODUCTION

Various applications based on the spin-exchange optical pumping of noble gas atoms have attracted extensive attention [1]. The nuclear spin polarization of noble gas atoms (e.g., Xe and Kr) are created by spin-exchange collisions with alkali-metal atoms (e.g., Rb and Cs), while the latter are polarized by circularly polarized laser beams. Polarized nuclear spins of noble gas atoms have been used to develop high-precision measurement devices including magnetometers for searching for extraordinary interactions of fundamental physics [2,3] and portable inertial measurement units [4,5]. Hyperpolarized noble gas was also used to implement diagnostic methods such as the magnetic resonance imaging (MRI) of lungs [6–8]. Also, the technology to produce liter volumes of hyperpolarized noble gas has been extensively discussed and developed [9–12].

The spin-exchange process plays crucial roles in the applications mentioned above. The spin-exchange rate determines the degree of the nuclear spin polarization of the noble atoms, which is essential to the signal-to-noise ratio (SNR) in MRI applications. The coherence time (e.g., the T_1 and T_2 times) of the polarized nuclear spins, which lies at the heart of high-precession measurement applications, is also affected by the spin-exchange process. In general, the spin-exchange rate depends on several key control parameters [13–19] including the density and the spin polarization of alkali-metal atoms, the magnetic field strength, and the pressure of the coexisting gas (e.g., the buffer gas). Understanding the mechanism of the spin-exchange process allows us to optimize these parameters and achieve better performance in applications.

The physical picture of the spin-exchange collision process was established theoretically and verified experimentally several decades ago [16,17]. In additional to the binary collision between a noble atom and an alkali-metal atom, for heavy noble gas atoms (e.g., Xe atoms), the spin-exchange process can occur in a bounded and relatively long-lived van der Waals (vdW) molecule formed by a noble atom, an alkali-metal atom, and a third-party atom or molecule. In this paper, we will focus on the spin-exchange process between Rb-Xe atoms in a vapor cell with N_2 buffer gas.

The binary collision and the vdW molecule process have distinguishing contributions to the spin-exchange rate at different control parameters. In the pioneering works, the role of vdW molecules were extensively studied with the buffer gas N_2 pressure ranging from a few Torr to $\approx$100 Torr [16,17], where the spin exchange within vdW molecules dominates the spin-exchange process. In the opposite limit, the spin-exchange rate due to binary collisions was experimentally determined in strong magnetic field ($\gtrsim$ 1 T) and high buffer gas pressure ($\gtrsim$1 atm) so that the vdW process was greatly suppressed [20–22].

Theoretical studies predicted that spin-exchange rate of the vdW molecule depends on the spin polarization of the alkali-metal atoms [16,18]. However, most of previous experimental studies focused on either the low-polarization [23] or high-polarization limits [21]. To our knowledge, a systematical measurement of the spin-exchange rate under different spin polarization is still absent. In this paper, we experimentally demonstrate the behavior of spin-exchange pumping of the Xe spins with well-calibrated Rb spin polarization. Our results provide a quantitative confirmation of the theoretical predication of the vdW process. More importantly, with the measurement of the spin-polarization dependence and the temperature dependence of the spin-exchange pumping rate, the key spin-exchange parameters due to the binary collision and the vdW process, together with the wall relaxation rate, can be separately extracted even when they have comparable contributions to the spin-exchange pumping rate.

*nzhao@csrc.ac.cn

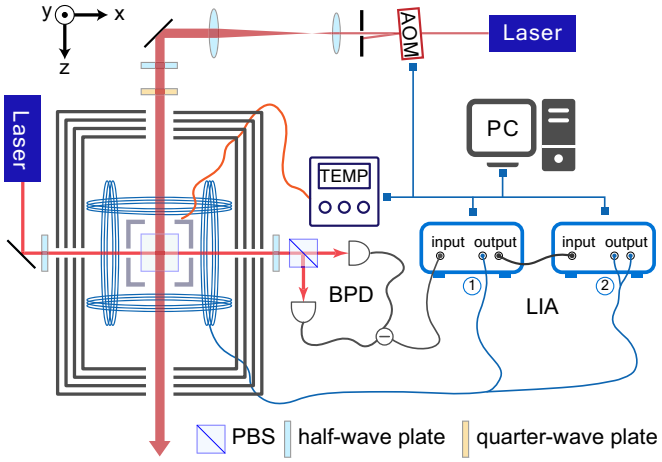

FIG. 1. Schematic illustration of the experiment setup. AOM, acousto-optic modulator; PBS, polarization beam splitter; BPD, balanced photodetector; LIA, lock-in amplifier.

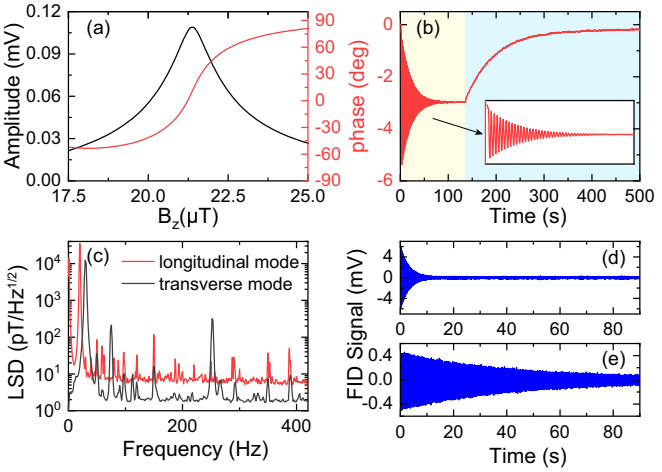

FIG. 2. Atomic magnetometer in longitudinal and transverse modes. (a) Amplitude and phase of ^{85}Rb magnetic resonance as functions of the bias field. The phase shift near the resonant point, which is linearly proportional to the change of the longitudinal field, is used to measure the Xe field along the z direction. (b) The longitudinal Xe field $b_S^z(t)$ of the Rabi nutation process (the data in yellow region and the inset) and the spin-exchange pumping process (the blue region). (c) Typical noise spectra of the atomic magnetometer in two modes. [(d), (e)] FID signals measured in the transverse mode with and without the pump beam, respectively.

Our measured results are in good agreement with the previous studies, and our study provides comprehensive evidences to the physical picture of spin-exchange optical pumping process.

This paper is organized as follows. In Sec. II, we introduce our experimental setup and measurement methods. Section III shows the experiment results. The conclusion is presented in Sec. IV.

II. EXPERIMENT SETUP AND METHOD

A. Experiment setup

Figure 1 shows a schematic of the experimental equipment. In our experiment, we measure the nuclear spin precession signal using a natural abundance Rb vapor cell of cubic shape with side length 1.0 cm. The cell, filled with 450 Torr N_2 buffer gas, 4 Torr ^{129}Xe, and 14 Torr ^{131}Xe noble gas, is enclosed in a boron-nitride oven. The oven is heated by a high-frequency (400 kHz) alternating electric current. A proportional integral derivative (PID) based temperature controller is used to maintain the cell temperatures, ranging from 70 to 120°C. The bias and the modulation magnetic fields along the z direction are created by two sets of Helmholtz coils. The magnetic fields in the transverse directions (x and y) are created by saddle coils. The oven and the coils are placed in a five-layer μ-metal magnetic shield. A σ^+-polarized pump beam with wavelength 795 nm (on resonance of the $D1$ line) along the z axis is applied to polarize the Rb atoms, and the Rb spin polarization is measured by the Faraday rotation effect of a linearly polarized probe beam with wavelength 780 nm (≈20 GHz detuned from the absorption peak of the $D2$ line) along the x axis. The Faraday rotation angle of the polarization plane of the probe beam is detected by a balanced photodetector and the signal is sent to two-stage cascade lock-in amplifiers. As discussed in the following section, the Rb spin is typically modulated by an RF magnetic field at a frequency of 100 kHz, and the bias field along z direction B_0 is set to the resonant point of ^{85}Rb spins [$B_0 = 21.3\,\mu$T; see Fig. 2(a)]. In the first stage (LIA-I), the signal is demodulated at the RF modulation frequency and the resulting signal is passed to the second stage (LIA-II), where the information of Xe nuclear spin precession is extracted.

B. Atomic magnetometer

The optically pumped Rb atoms create and detect the nuclear spin polarization of Xe atoms. The spin-polarized Rb atoms transfer their spin angular momenta to the Xe nuclear spins by spin-exchange collisions. The polarized Xe atoms cause an effective magnetic field $\mathbf{b}_S = b_{SK}\langle\mathbf{K}\rangle$, which is proportional to their nuclear spin polarization $\langle\mathbf{K}\rangle$ with a constant b_{KS}. The nuclear magnetic field $\mathbf{b}_S$ is sensed by the Rb atoms, which serve as an atomic magnetometer.

In this work, the Rb atomic magnetometer works in two different modes, namely, the longitudinal mode and the transverse mode. In the longitudinal mode, the Rb magnetometer measures the Xe field b_S^z along the z direction. This is achieved by applying a driving field along the y direction, whose frequency is in resonance with the ^{85}Rb Larmor precession frequency in the applied magnetic field. The Faraday rotation signal is then demodulated referenced to the driving field. In the absence of Xe field (i.e., $b_S^z = 0$), the exact resonance results in a zero demodulation phase [see Fig. 2(a)]. The Xe field b_S^z causes a frequency detuning and manifests itself as a nonzero phase shift. Within a reasonable range of $b_S^z \lesssim 100$ nT, the phase shift is proportional to the Xe field b_S^z.

Figure 2(b) shows an example of the application of the Rb magnetometer in the longitudinal mode. When the Xe spins are polarized along the z axis, we perform a Rabi nutation of the ^{129}Xe spins by applying a driving field in resonance with the ^{129}Xe Larmor frequency with a Rabi frequency ≈1 Hz. The longitudinal Rb magnetometer then records the change of the Xe field b_S^z [see Fig. 2(b)]. The nutation will eventually

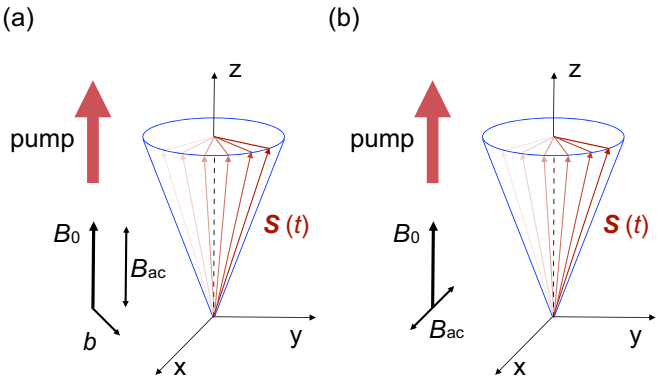

FIG. 3. Schematic of (a) transverse mode magnetometer and (b) longitudinal mode magnetometer. In both cases, B_0 is the bias field applied along the z direction, in parallel with the pump beam. The modulation field B_{ac} is applied along z and y directions for the transverse mode and the longitudinal mode, respectively. The transverse component $\langle S_x \rangle$ of Rb spins is detected by the Faraday rotation effect.

damp out after about ≈100 s and, at this moment, the Xe spins are almost depolarized with $\langle K_z \rangle \approx 0$. The driving field is then turned off and the Xe spin polarization will increase due to the spin-exchange pumping, which is, again, measured by the Rb magnetometer. With this measurement, we can obtain several important quantities characterizing the Xe spin dynamics, including the Xe polarization amplitude, the decay time of the Rabi nutation, and the spin-exchange pumping rate, which we are interested in this work. Particularly, this method is isotope selective, which allows us to study the properties of the two isotopes ^{129}Xe and ^{131}Xe independently even when they are coexisting in the cell.

In the transverse mode, the Xe field components b_S^x and b_S^y along x and y directions during the precession are detected. This is achieved by applying a modulation field along the z direction. If the transverse components b_S^x and b_S^y of the Xe field were zero, the Rb spin would be also aligned along the z direction due to the axial symmetry. In this case, the Faraday rotation detection would, of course, give a zero output signal. The presence of a nonzero transverse field b_S^x or b_S^y will tilt the Rb spin away from the z axis, giving rise to nonzero transverse components of Rb spin polarization $\langle S_x \rangle$ or $\langle S_y \rangle$. The amplitude and the direction of the Rb transverse polarization depend on the magnitudes of the transverse field to be detected. Furthermore, the Rb transverse polarization $\langle S_x \rangle$ and $\langle S_y \rangle$ will oscillate forced by the modulation field along the z direction (see Fig. 3). Thus, a modulated Faraday rotation angle signal at the RF modulation frequency will be detected by the balanced photodetector. In fact, this is a parametric oscillation process of spins, which was proposed and implemented to measure the field components perpendicular to the bias field [24]. Detailed theoretical treatment can be found in Ref. [4]. In Ref. [25], we also show that the transverse components b_S^x and b_S^y are obtained and distinguished by properly choosing the modulation amplitude and the demodulation phase. In our experiment, the sensitivity of the Rb magnetometer $<10\,\mathrm{pT}/\sqrt{\mathrm{Hz}}$ is achieved for both longitudinal and transverse modes, as shown in Fig. 2(c).

Figures 2(d) and 2(e) show two typical traces of the ^{129}Xe free-induction decay (FID) signal recorded by the transverse Rb magnetometer, from which the Larmor frequency of ^{129}Xe spins and the transverse spin decoherence time T_2 can be obtained. Particularly, we show that the Rb magnetometer works well even in the case that the Rb spins are very weakly polarized. Figure 2(e) demonstrates an FID signal with the pump beam blocked after polarizing the Xe spins. The Rb spin polarization is maintained at a very low level by the back polarization from the Xe spins. Although the FID signal is more than 10 times weaker than the normal case (with the pump beam), the signal-to-noise ratio is still good enough to obtain the Larmor frequency of Xe spins. This FID measurement in the absence of pump beam allows us to get rid of the influence of the Rb spin polarization and reveal the intrinsic dynamics of the Xe spin in the cell.

C. Spin-exchange rate and spin-relaxation rate

1. Spin-exchange interaction

The spin angular momentum transfer between Rb atom spin **S** and Xe atom spin **K** is caused by the spin-exchange interaction with the Hamiltonian

$$H_{\mathrm{ex}} = \alpha(R)\mathbf{S} \cdot \mathbf{K}, \tag{1}$$

where $\alpha(R)$ is the spin-exchange coupling strength, which is a function of the distance R between the alkali-metal atom and the noble gas atom. At high temperatures, the collision process is parametrized as a classical trajectory $R(t)$, and the interaction (1) becomes a time-dependent perturbation, $H_{\mathrm{ex}}[R(t)]$.

There are two types of collision processes, which have significantly different spin-exchange rates. Previous studies have shown that, in additional to the sudden binary collisions between Rb atoms and Xe atoms, the sticking collisions [14], in which Rb and Xe atoms form long-lived bounded molecules (vdW molecules), play an important role.

In general, two factors determine the spin-exchange rate of a given collision process, namely, (i) the probability of the collision and (ii) the amount of the spin state change during the collision. The former is usually related to the number densities of the atoms or molecules participating in the collision, while the latter depends on the *fluctuatuion* and the *correlation* of the interaction (1) at different times. Since the spin-exchange interaction (1) for two individual collision events are independent, nonzero correlation only occurs within the timescale of a single collision event. Thus, the typical collision time τ_c is a critical parameter in understanding the spin-exchange processes.

2. Binary collisions

Binary collisions have very short correlation time. Determined by the relative velocity $\approx 10^2$ m/s of the colliding atoms and the interaction range ≈Å of Eq. (1), the typical correlation time τ_c of binary collisions is on the order of $\approx 10^{-12}$ s. The short correlation time corresponds to a wide spectral bandwidth $\Delta\omega \approx 1/\tau_c \gg \omega_{\mathrm{hf}}$, or $\omega_{\mathrm{hf}}\tau_c \ll 1$, where $\omega_{\mathrm{hf}} \approx 2\pi \times 10^9$ Hz is the ground-state hyperfine splitting of Rb atoms. With this broad-band perturbation, the

spin-exchange interaction can induce the transition of Rb spin state with both $\Delta F = 0$ (within hyperfine levels with the same total angular momentum quantum number F) and $\Delta F = 1$ (between hyperfine levels with different F, e.g., $F = 2 \leftrightarrow F = 3$ for ^{85}Rb). References [16–18] have shown that, in this case, the spin-exchange rate is related to the fluctuations of the Rb *electronic* spin, $\langle S^2 - S_z^2 \rangle = 1/2$, which indeed is a constant. Thus, the spin-exchange rate due to the sudden binary collision is expressed as

$$\Gamma_{\text{bin}} = \langle \sigma_{\text{bin}} v \rangle n_A, \tag{2}$$

where n_A is the number density of the Rb atoms, which accounts for the collision probability, and $\langle \sigma_{\text{bin}} v \rangle$ is the velocity-averaged binary collision cross section, which quantifies the spin-exchange strength.

3. van de Waals molecule process

In the vdW molecule process, the Rb atom and Xe atom form a bounded pair, and the spin-exchange interaction can last as long as the lifetime τ_{m} of the vdW molecule, i.e., $\tau_{\text{c}} = \tau_{\text{m}}$. The mean molecule lifetime is measured as [26]

$$\tau_{\text{m}} = \frac{1.4\times10^{-7}\ \text{Torr s}}{p_{\text{N}_2}}, \tag{3}$$

where p_{N_2} is the pressure of the nitrogen buffer gas in unit of Torr. At very low N_2 pressure ($p_{\text{N}_2} \ll 100$ Torr), the N_2 molecules assist in the formation of the vdW molecules, and the spin relaxation rate due to vdW molecule is proportional to the N_2 pressure. Increasing the buffer gas pressure will increase the breakup rate of the vdW molecules and reduce the molecule lifetime. In the low pressure case (e.g., $p_{\text{N}_2} \approx 10^2$ Torr), the mean correlation time $\tau_{\text{c}} = \tau_{\text{m}} \approx 10^{-9}$ s, which is in the opposite limit ($\omega_{\text{hf}}\tau_{\text{c}} \gg 1$) to the binary collision case.

The spin-exchange strength of the vdW process is characterized by the rate [16–18]

$$\Gamma_\alpha = \frac{\phi_\alpha^2}{2T_{\text{vdW}}} \equiv \frac{n_{\text{A}}}{2n_{\text{N}_2}}\gamma_{\text{M}}, \tag{4}$$

where $T_{\text{vdW}}^{-1} = Z n_{\text{N}_2} n_A$ is the three-body molecule formation rate per Xe atom, with n_{N_2} and n_{A} being the densities of the N_2 buffer gas and the Rb atoms respectively, and the coefficient $Z = 5\times10^{-32}\ \text{cm}^{-6}\,\text{s}^{-1}$ [16]. In Eq. (4), ϕ_α^2 is the phase variances of ^{129}Xe spin precession caused by the Rb-Xe spin-exchange interaction in the vdW molecule process [18]. The variance is proportional to the squared vdW molecule lifetime, i.e., $\phi_\alpha^2 \propto \tau_{\text{m}}^2$. According to Eq. (3), we have $\phi_\alpha^2 \propto 1/p_{\text{N}_2}^2 \propto 1/n_{\text{N}_2}^2$. Thus, by canceling one n_{N_2} factor in the vdW molecule formation rate T_{vdW}^{-1}, we show that the spin-exchange strength Γ_α is proportional to the Rb density n_{A} and inversely proportional to the N_2 density n_{N_2}, with the proportional coefficient γ_{M}. In Eq. (4), a factor of 2 is explicitly defined to stay consistent with previous study [23].

As proposed by Zeng *et al.* [17], the coefficient γ_{M} is expressed in terms of several parameters which are independently determined as

$$\gamma_{\text{M}} = \frac{Z}{x^2}\left(\frac{p_0}{kT_0}\right)^2 = \frac{Z n_0^2}{x^2}, \tag{5}$$

where $x = 3.2$ is the Breit-Rabi parameter [16,17], $p_0 = 103$ Torr is the characteristic pressure of N_2 gas [16,17], and n_0 is corresponding the molecule density of N_2 at room temperature $T_0 = 300$ K. With these parameters, the rate γ_{M} is

$$\gamma_{\text{M}}^{(\text{Zeng})} = 5.4\times10^4\ \text{s}^{-1}. \tag{6}$$

In this paper, we will obtain the value of γ_{M} by the temperature and polarization measurements of the spin-exchange rate, and compare the result with Eq. (6).

Although Eq. (3) gives the *mean value* of the vdW molecule lifetime τ_{m}, the actual interaction time of each vdW molecules could have a distribution around the mean value. Appelt *et al.* have shown that the vdW molecule process can be divided into two coarse-grained groups with short and long correlation times [18]. In the following, we briefly review the different contributions of the short- and long-lived molecules to the spin-exchange rate.

Short-lived vdW molecules. The short-lived vdW molecules behave similarly to the binary collision case. Both $\Delta F = 0$ and $\Delta F = 1$ transitions can occur. The fraction of such short-lived vdW molecules is [18]

$$f_S = \frac{1}{1 + \omega_{\text{hf}}^2\tau_{\text{c}}^2}. \tag{7}$$

For a given buffer gas pressure and at a given cell temperature, the spin-exchange rate contributed by the short-lived vdW molecules is a constant regardless of the Rb spin polarization

$$\Gamma_{\text{vdW}}^{(S)} = f_S\Gamma_\alpha = \frac{f_S\gamma_{\text{M}}}{2n_{\text{N}_2}}n_A. \tag{8}$$

Long-lived vdW molecules. In long-lived vdW molecules, the interaction time is so long that the energy uncertainty of the vdW molecule is much smaller than the hyperfine splitting of the Rb atom. In this case, only the processes with $\Delta F = 0$ can occur in the long-lived vdW molecules, while the $\Delta F = 1$ processes are forbidden. The energy conservation requirement leads to the dependence of the spin-exchange rate on the population distribution of Rb hyperfine levels. Particularly, with the spin-temperature distribution, Appelt *et al.* shows that the vdW spin-exchange rate depends on the Rb spin polarization $P = 2\langle S_z \rangle$ via the function

$$\upsilon(P) = \sum_i \frac{\eta_i}{(2I_i+1)^2}[1 + \epsilon(I_i, P)] \tag{9}$$

for $i \in \{^{85}\text{Rb}, ^{87}\text{Rb}\}$, where η_i is the abundance of the Rb isotope i, I_i is the corresponding nuclear spin quantum number, and the so-called paramagnetic function is defined as

$$1 + \epsilon(I_i, P) = 2\langle \mathbf{F}\cdot\mathbf{F} - F_z^2 \rangle. \tag{10}$$

With the spin-temperature distribution, the expressions for ^{85}Rb ($I = 5/2$) and ^{87}Rb ($I = 3/2$) isotopes are [18]

$$1 + \epsilon\left(\frac{3}{2}, P\right) = \frac{5 + P^2}{1 + P^2}, \tag{11}$$

$$1 + \epsilon\left(\frac{5}{2}, P\right) = \frac{35 + 42P^2 + 3P^4}{3 + 10P^2 + 3P^4}. \tag{12}$$

Figure 4(b) demonstrates the dependence of $\upsilon(P)$ on the Rb spin polarization. The value of $\upsilon(P)$ will be reduced by

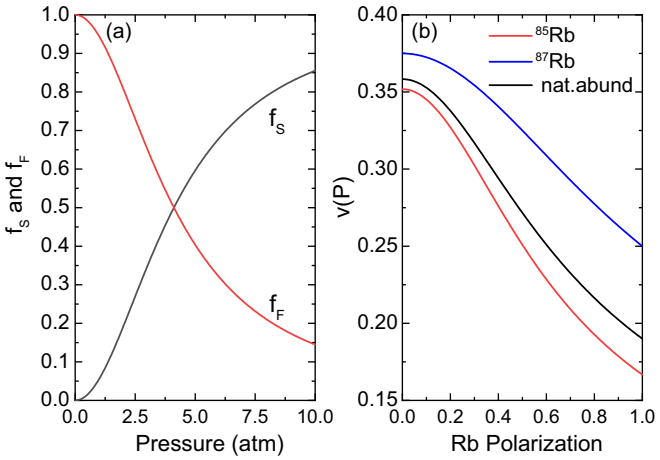

FIG. 4. (a) The relative ratios f_S and f_F of the S-damping and the F-damping processes as functions the buffer gas pressure, respectively. The molecular lifetime is estimated by Eq. (3), and ^{85}Rb hyperfine splitting $\omega_{\rm hf} = 2\pi \times 6.8$ GHz is used in the calculation. (b) The behavior of the $\upsilon(P)$ as a function of the Rb spin polarization P calculated by Eqs. (9), (11), and (12).

a factor of ≈2, if the Rb atoms changes from unpolarized ($P = 0$) to fully polarized ($P = 1$). Physically, this is reasonable since the function $\upsilon(P)$ indeed describes the Rb total spin fluctuations along the transverse directions (i.e., $\langle F_x^2 \rangle$ and $\langle F_y^2 \rangle$), as indicated in Eq. (10). Higher spin polarization P implies the Rb spins are better aligned along the z direction and then the transverse fluctuation is reduced.

With the fraction of long-lived vdW molecule

$$f_F = 1 - f_S = \frac{\omega_{\rm hf}^2 \tau^2}{1 + \omega_{\rm hf}^2 \tau^2}, \tag{13}$$

the spin-exchange rate due to the long-lived vdW molecules is

$$\Gamma_{\rm vdW}^{(F)} = f_F \Gamma_\alpha \upsilon(P) = \frac{f_F \gamma_{\rm M}}{2 n_{\rm N_2}} \upsilon(P) n_A \tag{14}$$

4. Spin-exchange pumping of Xe nuclear spins

With the spin-exchange rate due to binary and vdW molecules discuss above, the dynamics of the longitudinal component $\langle K_z \rangle$ of the Xe spins during the spin-exchange pumping process is governed by (see Eqs. (A33) and (A34) of Ref. [18])

$$\frac{d\langle K_z \rangle}{dt} = -(\Gamma_{\rm vdW} + \Gamma_{\rm bin} + \Gamma_{\rm w})\langle K_z \rangle + (\Gamma_{\rm vdW} + \Gamma_{\rm bin})\langle S_z \rangle, \tag{15}$$

where

$$\Gamma_{\rm vdW} = \Gamma_{\rm vdW}^{(S)} + \Gamma_{\rm vdW}^{(F)} = \Gamma_\alpha (f_S + \upsilon(P) f_F) \tag{16}$$

and $\Gamma_{\rm w}$ is the spin relaxation rate due to the cell wall. The wall relaxation of ^{129}Xe is independent of the Rb spin number density n_A and the spin polarization P. Furthermore, as shown in Fig. 4(a), in the low N_2 pressure case considered in this paper, $f_S \ll 1$ and $f_F \approx 1$. The long-lived molecules dominate the vdW process. In this case, the spin-exchange pumping rate becomes

$$\Gamma_{\rm ex} = \Gamma_\alpha \upsilon(P) + \Gamma_{\rm bin} + \Gamma_{\rm w}. \tag{17}$$

Before concluding this section, we discuss the physical picture of the spin-exchange pumping processes. As proposed by Happer *et al.*, the spin exchange between Rb and Xe atoms can be described by an RC circuit model [16,17]. The Rb atoms and Xe atoms are modeled as two capacitors $C_{\rm Rb}$ and $C_{\rm Xe}$ respectively, which are connected in parallel. The spin polarization $\langle F_z \rangle$ of Rb atoms and the nuclear spin polarization $\langle K_z \rangle$ of Xe play the role of charges. The Rb capacitor is charged by the circularly polarized beam, the battery, and then transfers its charge to the Xe capacitor. As shown in Eq. (143) of Ref. [16], in the long-lived vdW molecule process, the Rb capacitor is proportional to the transverse fluctuations of the total spin

$$C_{\rm Rb}^{(1)} \propto \langle F^2 - F_z^2 \rangle \propto 1 + \epsilon(I_i, P). \tag{18}$$

Indeed, the Rb capacitor itself is changing as it is charging the Xe capacitor. In contrast to the case described by Eq. (18), for the binary collision and the short-lived vdW processes, the interaction time is so short that the nuclear spins of Rb atoms do not respond. In this case, only the *electron spins* of Rb atoms are active in the processes, and the capacitor of Rb becomes

$$C_{\rm Rb}^{(2)} \propto \langle S^2 - S_z^2 \rangle = 1/2, \tag{19}$$

which is a constant independent of the spin polarization P. When the two types of spin-exchange processes (slow and fast) occur simultaneously, the Xe capacitor is charged by the two types of Rb capacitors $C_{\rm Rb}^{(1)}$ and $C_{\rm Rb}^{(2)}$ at the same time.

In summary, we have shown that the spin-exchange pumping consists of three different processes. The spin-exchange rate due the binary collision ($\Gamma_{\rm bin}$) and the vdW molecule process ($\Gamma_{\rm vdW}$) are proportional to the Rb density n_A. The latter also depends on the Rb spin polarization P. The wall-relaxation rate can be regarded as a constant. In the following, we show that these three different contributions to the spin-exchange rate are experimentally distinguished according to their n_A and P dependence.

III. RESULTS AND ANALYSIS

In this section, we present the measurement results and analysis of the spin-exchange and spin relaxation rates. We first measure the frequency shift of Xe spins induced by the polarized Rb atoms, which is used to calibrate the Rb spin polarization. We then discuss the spin-exchange rate of ^{129}Xe spins at different Rb spin polarization for a given cell temperature. The measurement data agree with the theoretical prediction quite well, which allows us to determine the rate $\Gamma_{\rm vdW}$. We finally study the temperature dependence of the spin-exchange rate. After subtracting the $\Gamma_{\rm vdW}$ contribution, we show that the remaining spin exchange rate is linearly proportional to the Rb spin density with a nonzero intercept, from which we determine the binary collision of the spin-exchange rate and the wall-relaxation rate. The spin-exchange and relaxation rates are also obtained by a three-parameter fitting process, which gives a better description of the measured spin-exchange pumping behavior.

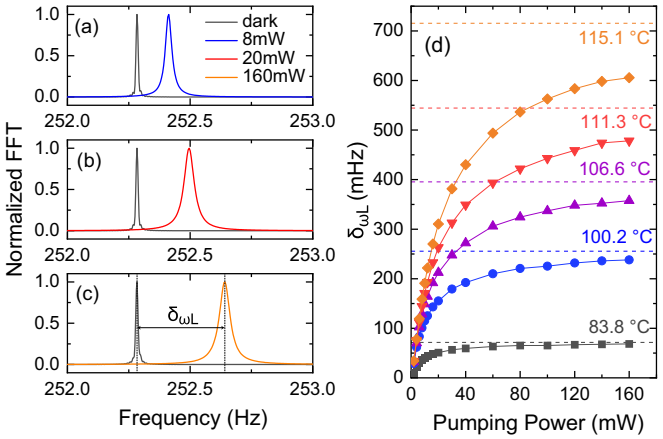

FIG. 5. [(a)–(c)] The FFT spectra of the FID signal of ^{129}Xe under various power of the pump beam. Compared to the signal in the absence of the pump beam (the black curves), the FID spectra in the presence of the pump beam (the red curves) are shifted and broadened. The frequency shift $\delta_{\omega L}$ and the peak width are increasing as increasing the power of the pump beam. (d) The frequency shift $\delta_{\omega L}$ of ^{129}Xe spins as a function of the pump power at different cell temperatures. The horizontal dashed lines indicate the saturated frequency shifts $\delta_{\omega L}^{(\infty)}$ in the case of fully polarized Rb spins at different temperatures (see text).

A. Calibration of Rb spin polarization

To study the Rb spin polarization dependence of the spin-exchange rate, we first calibrate the polarization. The polarized Rb spins will exert an effective magnetic field $\mathbf{b}_K = b_{KS}\langle\mathbf{S}\rangle$, which is proportional to the Rb spin polarization with a constant b_{KS}. In the longitudinal pumping case, the z component of the Rb effective field $b_K^z = b_{KS}\langle S_z\rangle = b_{KS}P/2$ causes a frequency shift $\delta\omega_L$ relative to the Larmor frequency determined by the applied static bias magnetic field B_0. We determine the frequency shift $\delta\omega_L$ by measuring the FID of the ^{129}Xe spins [see Fig. 5(a)]. Figure 5(b) shows the frequency shift $\delta\omega_L$ as a function of the power of the pump beam $P_{\rm inc}$ at various temperatures. In general, the frequency shift increases as pump power increases, and then is saturated in the large power limit. This is because the Rb spin polarization P depends on the optical pumping rate $R_{\rm op}$ as [27]

$$P = \frac{R_{\rm op}}{R_{\rm op} + R_{\rm rel}}, \tag{20}$$

where $R_{\rm rel}$ is the Rb spin relaxation rate. Since the optical pumping rate is proportional to the power of the incident pump beam, i.e., $R_{\rm op} = qP_{\rm inc}$ with a proportional coefficient q, we fit the measured frequency shift data by a model

$$\delta_{\omega L} = \delta_{\omega L}^{(\infty)} \frac{P_{\rm inc}}{P_{\rm inc} + P_{\rm rel}}, \tag{21}$$

where $\delta_{\omega L}^{(\infty)}$ is the saturated frequency shift and $P_{\rm rel} = qR_{\rm rel}$ is an effective power corresponding to Rb spin relaxation rate $R_{\rm rel}$. Indeed, the results shown in Fig. 5 agree with the polarization results obtained by measuring the transmission of the pump beam. However, the latter method may have large uncertainties when the optical depth (OD) of the cell is high (e.g., OD > 5) and meanwhile the pump power is low.

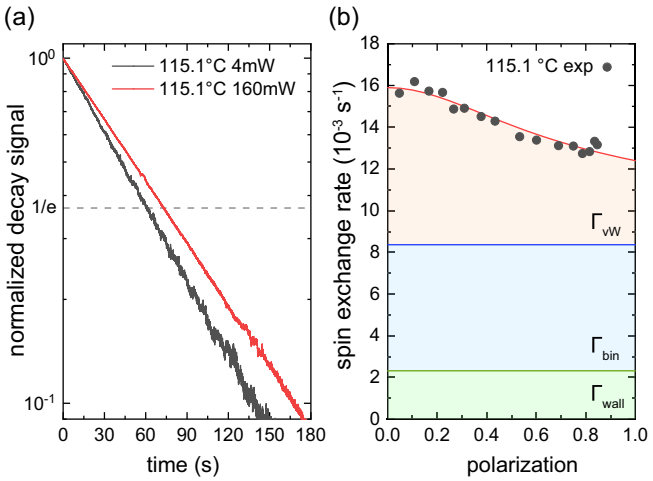

FIG. 6. (a) Two typical spin-exchange pumping processes with high (red curve) and low (black curve) Rb spin polarization respectively. (b) Measured spin-exchange pumping rate $\Gamma'_{\rm ex}$ (symbols) as a function of the calibrated Rb spin polarization. The red curve is the fitted result according to Eq. (17). From the fitting, three contributions $\Gamma_{\rm vdW}$, $\Gamma_{\rm bin}$, and $\Gamma_{\rm w}$ are extracted.

With the frequency shift measurement, the Rb spin polarization P at a given pump power and cell temperature is obtained by normalizing measured $\delta_{\omega L}$ of ^{129}Xe by the corresponding saturated value, i.e., $P = \delta_{\omega L}/\delta_{\omega L}^{(\infty)}$.

B. Polarization and temperature dependence of spin-exchange rate

Figure 6(a) shows two representative curves of the spin-exchange pumping process with different pump powers $P_{\rm inc}$ at temperature $T = 115.1$ °C, using the longitudinal mode Rb magnetometer and the measurement sequence demonstrated in Fig. 2(b). The pumping time increases from $T_{\rm ex} = 60.9$ to 73.1 s when increasing the pump power from $P_{\rm inc} = 4$ to 160 mW. As described by Eq. (14), this pump power dependence arises from the slow spin-exchange process within vdW molecules.

To have a quantitative understanding, we plot the spin-exchange rate $\Gamma'_{\rm ex} = T_{\rm ex}^{-1}$ versus the calibrated Rb spin polarization P in Fig. 6(b). By fitting the data (see the discussions below), we distinguish the vdW molecule and the binary collision contributions to the spin-exchange rate, together with the wall-relaxation rate. Unlike the low N_2 pressure ($p_{N_2} <$ 100 Torr) case [17], our measurement shows the binary collision (the blue region) and the vdW molecule process (the orange region) have comparable sizes in a cell with higher N_2 pressure ($p_{N_2} = 450$ Torr).

We analyze the measured data by two fitting models. First, we use the vdW molecule parameters in Eqs. (5) and (6) determined by Zeng *et al.* in Ref. [17] and extract the two unknown parameters $\langle\sigma_{\rm bin}v\rangle$ and $\Gamma_{\rm w}$ from our measurement data. Figure 7(a) shows the spin-exchange pumping rates as functions of the Rb spin polarization at different temperatures. The dependence on the Rb spin polarization of the spin-exchange rate becomes more significant with increasing Rb density. With the fixed value of $\gamma_{\rm M}^{\rm (Zeng)}$ in Eq. (6),

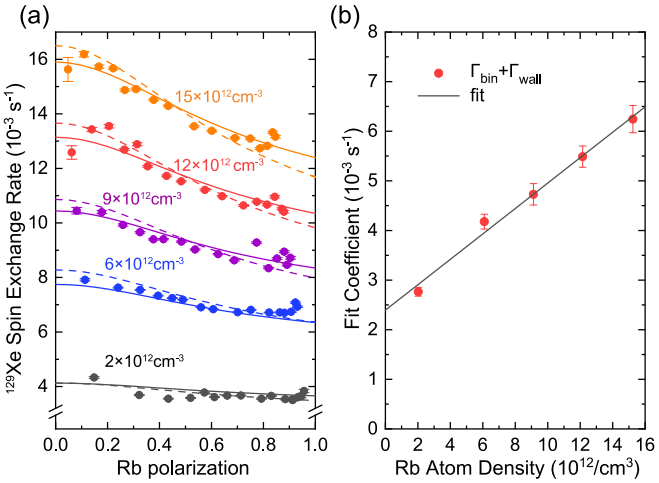

FIG. 7. (a) The measured spin-exchange pumping rates (symbols) at different temperatures and the two-parameter (dashed curves) and three-parameter (solid curves) fitting results according to Eq. (17). (b) The pump-power-independent rate (i.e., $\Gamma_{\rm bin}+\Gamma_{\rm w}$) is linearly proportional to the Rb atom density, from which the binary collision cross section and the wall-relaxation rate are determined.

the polarization-independent rates $\Gamma_{\rm bin}+\Gamma_{\rm w}$ are obtained by deducting the vdW molecule contribution from the measured total rates at different temperatures [see Fig. 7(b)]. A simple two-parameter linear fitting of the rate $\Gamma_{\rm bin}+\Gamma_{\rm w}$ versus the Rb spin density $n_{\rm A}$ gives the two-body spin-exchange parameter and the wall-relaxation rate as

$$\begin{aligned}\langle\sigma_{\rm bin}v\rangle^{(2p)} &= (2.56\pm0.49)\times10^{-16}\,{\rm cm}^3\,{\rm s}^{-1},\\ \Gamma_{\rm w}^{(2p)} &= (2.40\pm0.49)\times10^{-3}\,{\rm s}^{-1}.\end{aligned}\tag{22}$$

An alternative fitting process is performed by regarding vdW parameter $\gamma_{\rm M}$, the binary collision parameter $\langle\sigma_{\rm bin}v\rangle$, and the wall relaxation rate $\Gamma_{\rm w}$ as three independent adjustable parameters. The three-parameter fitting results are shown by the solid curves in Fig. 7(a) with

$$\begin{aligned}\gamma_{\rm M}^{(3p)} &= (3.95\pm0.34)\times10^{4}\,{\rm s}^{-1},\\ \langle\sigma_{\rm bin}v\rangle^{(3p)} &= (4.02\pm0.35)\times10^{-16}\,{\rm cm}^3\,{\rm s}^{-1},\\ \Gamma_{\rm w}^{(3p)} &= (2.32\pm0.13)\times10^{-3}\,{\rm s}^{-1},\end{aligned}\tag{23}$$

which indicates a slightly lower (higher) value of the vdW molecular (binary) contribution than the two-parameter fitting result. Although the two-parameter fitting based on previous parameters [17] already gives a satisfactory description of the polarization-dependence behavior [the dashed curves in Fig. 7(a)], the three-parameter fitting results in Eq. (23) show a better agreement to our measured data.

The binary collision parameter $\langle\sigma_{\rm bin}v\rangle$ obtained by the three-parameter fitting is very close to the previous results [17,23] measured in similar conditions. Some other measurements [20–22,28] performed in strong magnetic fields (>1 T) and high gas pressures (>1 atm) gave the binary parameters in the same order. The spread values in these measurements, ranging from 1.75×10^{-16} [21] to $10\times10^{-16}\,{\rm cm}^3\,{\rm s}^{-1}$ [22], may arise from the different magnetic fields and, more possibly, from the calibration of the density of alkali atoms. The vdW molecule parameter $\gamma_{\rm M}^{(3p)}$ obtained in our work is also close to the result $\gamma_{\rm M}^{(\rm Zeng)}$ estimated in Ref. [17]. The ≈30% difference may attribute to the temperature dependence of the parameters, e.g., Z and p_0.

IV. CONCLUSION

In this paper, we study the spin-exchange rate between optically pumped Rb atoms and the Xe atoms. We experimentally demonstrate the dependence of the spin-exchange rate on the Rb spin polarization. We measure the spin-exchange parameters of the vdW molecule process and the binary collision process in the regime where the two processes have comparable contributions to the total spin-exchange rate. Our work provides a direct confirmation of the theoretical prediction (i.e., the polarization dependent behavior of the spin-exchange rate) and gives the spin-exchange parameters in good agreement with previous studies.

ACKNOWLEDGMENTS

We thank Prof. Dong Sheng for providing the vapor cell and for the inspiring discussions. This work is supported by National Basic Research Program of China (Grant No. 2016YFA0301201) and NSAF (Grants No. U1930402 and No. U2030209).

[1] T. G. Walker and W. Happer, Rev. Mod. Phys. **69**, 629 (1997).
[2] M. Bulatowicz, R. Griffith, M. Larsen, J. Mirijanian, C. B. Fu, E. Smith, W. M. Snow, H. Yan, and T. G. Walker, Phys. Rev. Lett. **111**, 102001 (2013).
[3] J. Lee, A. Almasi, and M. Romalis, Phys. Rev. Lett. **120**, 161801 (2018).
[4] T. G. Walker and M. S. Larsen, Adv. At. Mol. Opt. Phys. **65**, 373 (2016).
[5] D. Budker and M. Romalis, Nat. Phys. **3**, 227 (2007).
[6] G. Collier, T. Pałasz, A. Wojna, B. Głowacz, M. Suchanek, Z. Olejniczak, and T. Dohnalik, J. Appl. Phys. **113**, 204905 (2013).
[7] J. P. Mugler and T. A. Altes, J. Magn. Reson. Imaging **37**, 313 (2013).
[8] H. E. Möller, X. J. Chen, B. Saam, K. D. Hagspiel, G. A. Johnson, T. A. Altes, E. E. De Lange, and H. U. Kauczor, Magn. Reson. Med. **47**, 1029 (2002).
[9] B. Hersman, in *Proceedings of the XVth International Workshop on Polarized Sources*, PoS (PSTP2013) 063, Charlottesville, Virginia.
[10] M. S. Freeman, K. Emami, and B. Driehuys, Phys. Rev. A **90**, 023406 (2014).
[11] P. Nikolaou, A. M. Coffey, L. L. Walkup, B. M. Gust, N. Whiting, H. Newton, S. Barcus, I. Muradyan, M. Dabaghyan, G. D. Moroz, M. S. Rosen, S. Patz, M. J. Barlow, E. Y. Chekmenev, and B. M. Goodson, Proc. Natl. Acad. Sci. USA **110**, 14150 (2013).
[12] G. Schrank, Z. Ma, A. Schoeck, and B. Saam, Phys. Rev. A **80**, 063424 (2009).

[13] M. A. Bouchiat, J. Brossel, and L. Pottier, Phys. Rev. Lett. **19**, 817 (1967).
[14] C. C. Bouchiat, M. A. Bouchiat, and L. C. L. Pottier, Phys. Rev. **181**, 144 (1969).
[15] M. A. Bouchiat, J. Brossel, and L. C. Pottier, J. Chem. Phys. **56**, 3703 (1972).
[16] W. Happer, E. Miron, S. Schaefer, D. Schreiber, W. A. van Wijngaarden, and X. Zeng, Phys. Rev. A **29**, 3092 (1984).
[17] X. Zeng, Z. Wu, T. Call, E. Miron, D. Schreiber, and W. Happer, Phys. Rev. A **31**, 260 (1985).
[18] S. Appelt, A. B.-A. Baranga, C. J. Erickson, M. V. Romalis, A. R. Young, and W. Happer, Phys. Rev. A **58**, 1412 (1998).
[19] I. A. Nelson and T. G. Walker, Phys. Rev. A **65**, 012712 (2001).
[20] M. P. Augustine and K. W. Zilm, Chem. Phys. Lett. **280**, 24 (1997).
[21] Y. Y. Jau, N. N. Kuzma, and W. Happer, Phys. Rev. A **66**, 052710 (2002).
[22] W. Shao, G. Wang, and E. W. Hughes, Phys. Rev. A **72**, 022713 (2005).
[23] G. D. Cates, R. J. Fitzgerald, A. S. Barton, P. Bogorad, M. Gatzke, N. R. Newbury, and B. Saam, Phys. Rev. A **45**, 4631 (1992).
[24] Z. Li, R. T. Wakai, and T. G. Walker, Appl. Phys. Lett. **89**, 134105 (2006).
[25] F. Tang, A.-X. Li, K. Zhang, Y. Wang, and N. Zhao, J. Phys. B: At. Mol. Opt. Phys. **52**, 205001 (2019).
[26] N. D. Bhaskar, W. Happer, M. Larsson, and X. Zeng, Phys. Rev. Lett. **50**, 105 (1983).
[27] S. J. Seltzer, *Developments in Alkali-Metal Atomic Magnetometry* (Princeton University Press, Princeton, NJ, 2008).
[28] Z. Liu, M. Zhao, C. Wu, L. Li, S. Li, X. Zeng, and W. Xiong, Chem. Phys. Lett. **194**, 440 (1992).